



Long-term hydrochemical monitoring and geothermometry: understanding groundwater salinization and thermal fluid contamination in Mila's basin, Northeastern Algeria

Yasmina Bouroubi-Ouadfel¹ · Adnane Souffi Moulla² · Abdelkader Khiari¹

Received: 23 August 2023 / Revised: 23 October 2023 / Accepted: 22 November 2023 / Published online: 15 December 2023
© The Author(s), under exclusive licence to Science Press and Institute of Geochemistry, CAS and Springer-Verlag GmbH Germany, part of Springer Nature 2023

Abstract The regular hydrochemical monitoring of groundwater in the Mila basin over an extended period has provided valuable insights into the origin of dissolved salts and the hydrogeochemical processes controlling water salinization. The data reveals that the shallow Karst aquifer shows an increase in TDS of 162 mg L^{-1} while the thermal carbonate aquifer that is also used for drinking water supply exhibits an increase of 178 mg L^{-1} . Additionally, significant temperature variations are recorded at the surface in the shallow aquifers and the waters are carbogaseous. Analysis of dissolved major and minor elements has identified several processes influencing the chemical composition namely: dissolution of evaporitic minerals, reduction of sulphates, congruent and incongruent carbonates' dissolution, dedolomitization and silicates' weathering. The hydrogeochemical and geothermometric results show a mixing of saline thermal water with recharge water of meteoric origin. Two main geothermal fields have been identified, a partially evolved water reservoir and a water reservoir whose fluid interacts with sulphuric acid (H_2S) of magmatic origin. These hot waters that are characterized by a strong hydrothermal alteration do ascend through faults and fractures and contribute to the

contamination of shallower aquifers. Understanding the geothermometry and the hydrogeochemistry of waters is crucial for managing and protecting the quality of groundwater resources in the Mila basin, in order to ensure sustainable water supply for the region. A conceptual model for groundwater circulation and mineralization acquisition has been established to further enhance understanding in this regard.

Keywords Hydrochemical monitoring · Hydrogeochemistry · Salinization · Geothermal reservoir · Contamination · Mila's basin

1 Introduction

In semi-arid and arid regions groundwater over-pumping driven by both an increasing demand and climate change, has led to deeper extraction levels. This resulted in the overexploitation of aquifers and the contamination of water resources with various pollutants. Groundwater salinization, that is characterized by increased dissolved salt concentrations, has emerged as a significant form of pollution, adversely affecting groundwater quality. Several researchers have studied the origins of salinity and the processes of groundwater mineralisation acquisition. Indeed, potential sources of salinity in waters are: dissolution of evaporite minerals (Cardenal et al. 1994; Moussa et al. 2011; Khaska et al. 2013), saltwater intrusion from sabkhas (Farid et al. 2013; Demdoum et al. 2015; Dhaoui et al. 2023), intrusion of fossil marine water that is trapped in sediments (Barbecot et al. 1998; Vallejos et al. 2018; Cherchali et al. 2023), current marine intrusion (Custodio and Bruggeman 1987; Bouchaou et al. 2008; Martínez-

Adnane Souffi Moulla is a retired scientist of Algiers Nuclear Research Centre.

✉ Adnane Souffi Moulla
asmoulla@gmail.com

¹ Natural Resources and Management of Sensitive Environments Lab, Geology Department, Oum El Bouaghi University, 04000 Oum El Bouaghi, Algeria

² Dating and Isotope Tracing Department, Algiers Nuclear Research Centre, 16000 Algiers, Algeria

Pérez et al. 2022), upwelling of deep saline water from the basement (Frape et al. 1984; Aquilina et al. 2002; Hébrard et al. 2006; Walter et al. 2017), agricultural activities (Stigter et al. 1998; Pulido-Bosch et al. 2018) and saline pollution caused by the infiltration of mining brines (Lucas et al. 2010).

In Mila's province, which is located approximately 70 km south of the Mediterranean Sea, groundwater serves as the exclusive source of drinking water supply and irrigation for numerous municipalities, despite the presence of the large Beni Haroun dam (960 hm³ capacity). The dam's water is primarily allocated to major cities in eastern Algeria, such as Constantine, Jijel, Mila (city center), Oum El Bouaghi, Batna, and Khenchela (ANBT 2000). In the central zone of Mila's prefecture, traditional wells and more than 51 permanent springs used to be the primary sources of drinking water before the 1960s (DHW Mila 1996). The drilling of boreholes in the region started in 1980, primarily in the Boussellah valley. In the 2000s, the number of boreholes increased significantly to meet agricultural demand for irrigation water. By 2008, the number of springs has decreased to only a dozen with temporary flow that were productive only during winter seasons (ADE Mila 2013). In 2019, 32 boreholes were producing over 400 L·s⁻¹, with a pumping duration of 18 h per day, exclusively for drinking water supply (DHW of Mila 2020). On a province-wide scale, there were 306 boreholes and 928 wells used for irrigation (Agricultural Services Directorate of Mila 2020). The cultivated land surface area in the province of Mila extends over ~ 248.454 hectares (DSASI 2021), with groundwater being the primary source of water for irrigation. The groundwater quality monitoring network operated by the National Water Resources Agency of Constantine in the Mila region started in 1993 and continued until 2012. It concerned five drinking water supply boreholes in different prefectures. During almost two decades of excessive pumping, hydrochemical monitoring showed a clear increase in total mineralisation and excessive nitrate levels. The hydrogeological complex in the central part of Mila's province has been the focus of our investigation and involved a regular hydrochemical monitoring of groundwater over a decade and encompassing three boreholes. During this period, significant changes have been observed including an increase in total dissolved mineralization, elevated bicarbonate levels, and a wide range of groundwater temperatures. Furthermore, the study area is characterized by the presence of six natural thermal springs, out of the ten in Mila's province (Issadi 1992; Dib 2008), located close to the boreholes used for drinking water supply, including one directly exploited through drilling. All these thermal springs are characterized by a continuous flow.

Based on these observations and the notable physico-chemical and hydrochemical variations, our investigation aims to achieve the following objectives:

- Determine the potential sources of water salinization
- Identify the hydrogeochemical processes responsible for water salinization
- Define the various origins of the pollution affecting the groundwater
- Investigate and characterize the thermal aquifer in the basin, including its depth and temperature
- Explore the relationship between the thermal aquifer and the shallow aquifer used for drinking water supply
- Identify potential mixings within the groundwater
- Establish a water circulation model for the hydrogeological complex.

The overarching goal of this study is to develop a conceptual model explaining groundwater circulation and salinization in the multi-layer aquifer complex of the central basin. By understanding the origins and by highlighting different pollution sources affecting groundwater, our research aims at preventively contributing to raise awareness about groundwater quality degradation. This effort is crucial in preventing a dysfunction of the aquifer complex and in promoting the sustainability of water resources. Additionally, targeting the thermal aquifer could provide insights into its geothermal potential.

1.1 Study area

Mila's province is located in the north-east of Algeria, about 50 km north-west of Constantine. The study area constitutes the central part of Mila's province, the southern zone of the El Kebir–Enndja wadis sub-watershed (Fig. 1). The region is characterized by a very varied terrain. In the north, high altitude mountains such as Jebel El Halfa (1155 m) and Jebel Ouakissen (1045 m) are found. Plains with altitudes ranging from 400 to 650 m occur in the central part. The southern part is characterised by the presence of another mount namely Koudiat Touachra (1000 m) and Jebel El Kenazaa (1082 m) whereas to east occurs Jebel Lakhhal (1256 m). The climate is semi-arid (Mebarki 2005). Rainfall varies between 400 and 600 mm year⁻¹ (ANRH 2005). The average air temperature is 15.5 °C (ONM 2013). The average evapotranspiration is 1151 mm year⁻¹ (ANRH 2003). The economy of the region depends mostly on agriculture (cereals crops). Mila's province is crossed from west to east by El Kebir wadi which together with both Boussellah and Maleh wadis forms Endja wadi. The latter is 78 km long (Fig. 1) and has a flowrate of 3.26 m³ s⁻¹ (ABH 2004). The Boussellah and Maleh wadis have a temporary flow and are characterised by strong floods during autumn and spring and drain all the

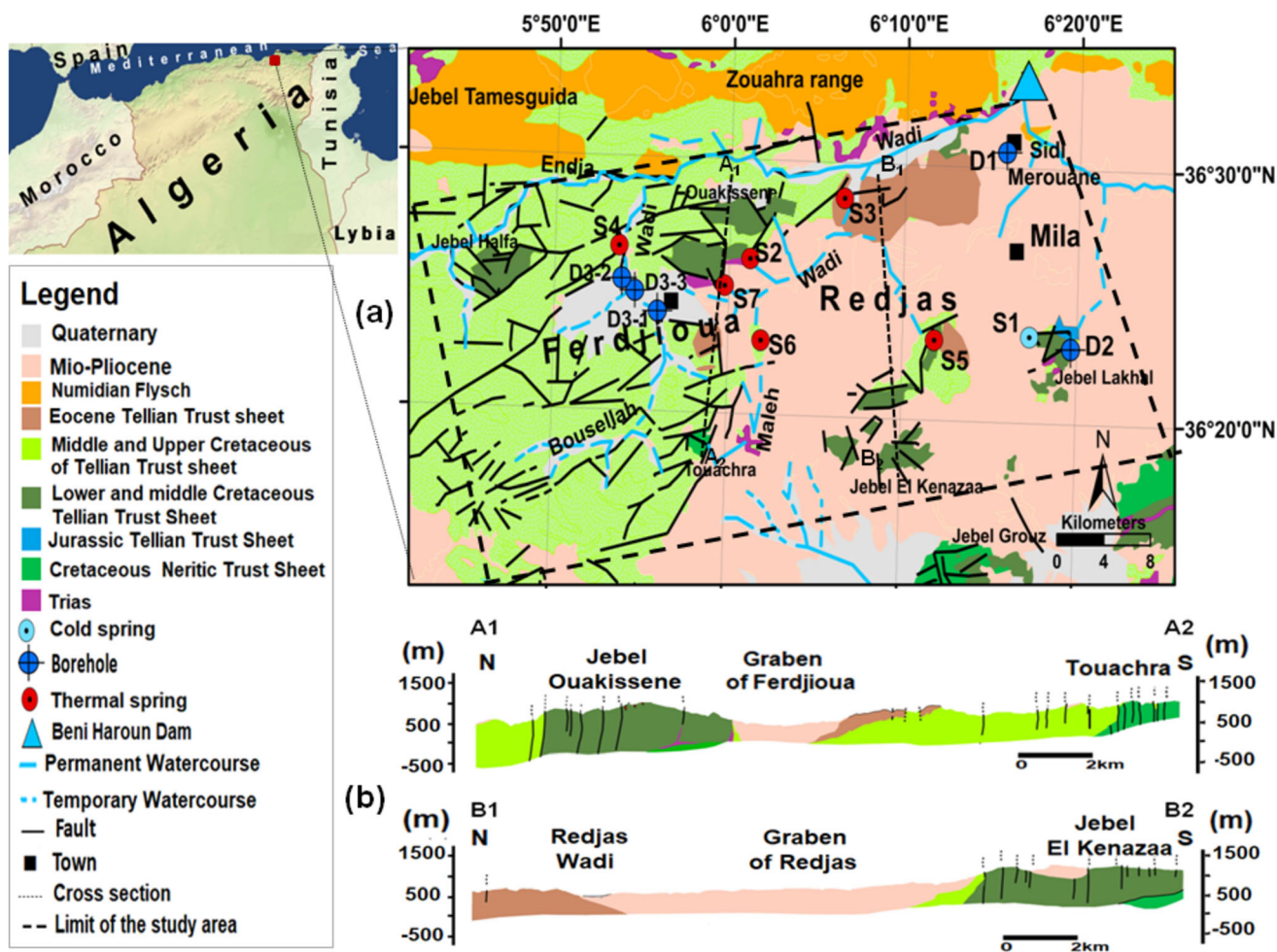


Fig. 1 a Simplified geological map and location of sampled water point; b Geological cross-section showing the main tectonic structures

water from the southern slopes of the neighbouring hills. The basin is characterised by an important and aggressive torrential drainage (Mebarki 2005).

1.2 Geological and hydrogeological settings

The study area is contained within the external domain of the Maghrebide's range which is a set of southern vergence thrust sheets formed during the Tertiary era (Durand-Delga 1969; Wildi 1983; Benaouali-Mebarek et al. 2006). The external domain includes the allochthonous Tellian series, the allochthonous foreland series and the autochthonous Atlasian foreland series (Vila 1980). The Tellian allochthonous formations are composed of a thick series of Mesozoic carbonates (alternating limestone, limestone-marly and marl) (Vila 1980). This is the domain that makes up the majority of the study region (Fig. 1). The external domain is overlapped to the north by the Flysch-sheet of Numidian sandstones and clays. The extrusive Triassic layers that are composed of multicoloured clays, crushed gypsum and dolomitic limestone icicles mark out the

anomalous contacts that delineate the carbonates extensions. The Eocene sediments are composed of massive limestone and marl. The Mio-Pliocene formations are made of clays with salt intercalations, conglomerates and lacustrine limestones (Vila 1980; Coiffet 1992). The Quaternary formations consist of alluvia, gravels, sand, sandy clay and marl (Fig. 1). Two Neogene collapse ditches characterize the structural geomorphology of the region namely Ferdjioua and Redjas grabens (Vila 1980; Coiffet 1992). In addition to the SW–NE kilometric faults inherited from very ancient tectonic phases; the region is also affected by intense neotectonic activities that gave birth to north–south trending faults that affect the Mio-Plio-Quaternary formations (Aris et al. 1998; Benabbas 2006) as well as the presence of a strong seismic activity (Yelles-Chaouch et al. 2021; Tebbouche et al. 2022).

The hydrogeological complex of the study area is a multi-layered set of Mesozoic marly limestones and marlstones, underlying the continental and Quaternary Mio-Pliocene superficial sediments' cover. The characteristics of the sediments and the structure of the land determine the

location of the aquifers. The permeable Quaternary alluvium is well extended along the Endja and Boussellah wadis. Moreover, the fractured carbonates of the Mesozoic have developed important karstic aquifers, and the fissured sandstones of the Numidian nappe are also aquiferous in some places. The different aquifers formations of the studied basin are summarised in Table 1.

Spring S1 emerges in the north–western part of Jebel Lakhal (1256 m) at an altitude of 914 m in the Mesozoic carbonates. The shallow Karstic aquifer that is contained in the Cretaceous formations of the region of Sidi Merouane (Vila 1980) is known through a few boreholes. The karstified formations occurring in a shallow horst structure under the Mio-Pliocene sediments constitute a significant water reservoir. Borehole D1 crosses the roof of the karstified limestones at a depth of 10 m while the saturated zone is reached at 26 m. The well-developed karstification of these carbonates makes the aquifer resource sensitive to point–source pollution. Borehole D2 taps the thermal spring which emerges from the karstified limestones of Jebel Lakhal. This first borehole drilled in 1990 at a few meters of the thermal spring is still artesian (except during pumping when the dynamic level reaches 1.5 m). The Quaternary alluvial aquifer in Ferdjioua graben is a semi-confined system that is exploited by more than twenty boreholes all located along the valley of Boussellah wadi. The thickness of the alluvium varies between 20 and 50 m. They are surmounted by slightly sandy clay formations (4–20 m) and have marl as a substratum. Data from pumping tests show an average permeability ($K = 4 \times 10^{-2} \text{ m s}^{-1}$). The overall flow rate pumped from the valley is almost 200 L s^{-1} (DHW Mila 2013), (D3-1, D3-2 and D3-3) are the boreholes used in this study. Thermal water S2 emerges near Jebel Hadid close to a

SW–NE fault in the Mesozoic carbonates. Spring S3 emerges 150 m from the left bank downstream of Maleh wadi. The thermal water S4 is located near the edge of Ferdjioua's trough. It emerges on the left bank of Boussellah wadi, close to a SW–NE fault (Fig. 1). Thermal spring S5 emerges through the Redjas graben in a ravine. Thermal water S6 emerges from the Maastrichtian limestone formations in a ravine in the upstream area of Maleh wadi. Thermal water S7 emerges at the intersection of two faults (directed E–W and N–S) which are boundary faults of Jebel Boucheref. The E–W fault fractures are filled with Triassic formations. The waters of S2 and S7 flow into the course of El Maleh wadi in the southern area where this ephemeral watercourse crosses superficial formations of the Triassic evaporites (Fig. 1).

2 Materials and methods

More than sixty water samples were collected from drillings D1, D2 and D3-1 (Table 1) whose water is up to the present date used as drinking water. These boreholes were part of the hydrochemical groundwater monitoring network operated by the National Agency for Water Resources (ANRH) from (1993 to 2012). This network consisted of fifty boreholes from this North–Eastern region of Algeria, and all the achieved analyses are recorded in Siqueau software and constitute a database. The hydrochemical monitoring of D1 and D2 boreholes' waters covered the period ranging from 1993 to 2011, while that of D3-1 covered only the period from 2000 to 2011.

In the present work, we used the monitoring period that is common to the three boreholes, in addition to the 1993 data and 1994 data respectively for the waters of D1 and

Table 1 Aquifer formations and water points features used in this study

Water point	Aquifer	Flow rate ($\text{L}\cdot\text{s}^{-1}$)	Depth (m)	Altitude (m)	Observation
S1	Shallow Cretaceous Karst limestone	0.04	–	914	Temporary flow
D1	Shallow Cretaceous Karst limestone	25	48	350	–
D2	Thermal Aquifer	33	210	555	–
D3-1	Detrital aquifer Quaternary alluvium	12	40	498	–
D3-2	Detrital aquifer Quaternary alluvium	25	50	482	–
D3-3	Detrital aquifer Quaternary alluvium	12	50	490	–
S2	Thermal Aquifer	2	–	526	Permanent flow
S3	Thermal Aquifer	1	–	218	Permanent flow
S4	Thermal Aquifer	3	–	477	Permanent flow
S5	Thermal Aquifer	1.5	–	500	Permanent flow
S6	Thermal Aquifer	1	–	512	Permanent flow
S7	Thermal Aquifer	2	–	525	Permanent flow

D: Drilling, S: Spring. D1, D2, D3-1, D3-2 & D3-3 are used for drinking water, S2, S4, S5 & S7 are used for spa (Hamman)

D2 boreholes. We used 13 samples from borehole D1, 11 samples from borehole D2 and 18 samples data from borehole D3-1. Chemical analyses of the water from D3-2 and D3-3 were carried out at the end of the work on these boreholes in 2010 and 2013 respectively. The waters of the temporary springs were subject to hydrochemical analyses once their flowrate became significant. The hydrochemical data for the boreholes' water was obtained from the ANRH database (Table 2). During 2012, we took samples of thermal waters throughout the province of Mila which concerned the central zone; six water points were concerned. Temperature (T °C), hydrogen potential (pH) and electrical conductivity (EC) were measured in-situ for each sample. The major chemical elements that were analyzed are: Ca^{2+} , Mg^{2+} , Na^+ , K^+ , HCO_3^- , Cl^- , SO_4^{2-} and NO_3^- with an ionic balance of about $\pm 5\%$. These chemical elements were analyzed at the ANRH laboratory in Constantine. Silica (SiO_2) were analyzed in the Algiers ANRH-Laboratory. Air temperature data were collected from the Office National de Météorologie of Constantine (ONM–National Meteorology Office). In order to better understand the hydrochemical processes taking place in thermal aquifers and due to the lack of trace element results, we used strontium (Sr) and lithium (Li) data from the work of Ferraga and Pistre (2021), Bromine (Br) contents were obtained from the work of Issadi (1992) and Amarouche-Yala et al. (2014).

The hydrogeochemical facies were determined based on Piper classification (1944) and Langelier–Ludwig diagram (1942). TDS was determined by the software “Diagrammes” (Simler 2014) from all the parameters measured in situ and the composition of the chemical elements analyzed. The binary plots between chemical elements were drawn making use of Excel software from a Microsoft Office suite. The variables of the equilibrating carbon dioxide partial pressure (P_{CO_2}) and saturation indices (SI) with respect to anhydrite, gypsum, halite, calcite, dolomite, aragonite, talc and other minerals were calculated using the geochemical software (Phreeqci-3.1.4–8929) developed by Parkhurst and Appelo (2013). The Giggenbach Na–K–Mg (1988) and $\text{Cl–SO}_4\text{–HCO}_3$ (1991) diagrams are used to classify different types of thermal waters. Those diagrams were produced using Excel spreadsheets by Powell and Cumming (2010) (Liquid_Analysis_v1_Powell-2010-StanfordGW.xls). The main chemical geothermometers (silica and cations) are applied to determine the temperature and the depth of the thermal reservoir.

3 Results and discussion

The measured physico-chemical parameters of the analyzed samples are presented in Table 2. The physical and chemical parameters of the groundwater in the study area are highly variable in time and space. The water groups were established on the basis of the Total Dissolved Solutes (TDS) content (Davis and De Wiest 1967) and waters' temperature classifications of Gosselin and Schoeller, 1939 in (Castany 1963). According to Davis and De Wiest (1967), freshwater has a $\text{TDS} < 1 \text{ g L}^{-1}$, brackish water $1 \text{ g L}^{-1} \leq \text{TDS} \leq 10 \text{ g L}^{-1}$ and saline water $\text{TDS} > 10 \text{ g L}^{-1}$. According to Gosselin and Schoeller (1939), a thermal water is defined as a water whose temperature exceeds the average annual air temperature by more than 5 °C. The mean annual ambient temperature for Mila's region is 15.5 °C (ONM 2013). Referring to the aforementioned definition for thermal waters, every groundwater within the province whose temperature exceeds 20.5 °C should be considered as a thermal one. Knowing that the depth of all the boreholes is between 40 and 210 m, the geothermal gradient in Mila's province is 3.85 °C (Kedaid 2007; Chenaker et al. 2018). According to the groundwater classification made by Castany (1963), cold water temperatures are < 20 °C; hypothermal waters temperatures are in the range: 20 °C $\leq T \leq 35$ °C. Mesothermal waters' temperatures fall in the range: 35 °C $\leq T \leq 50$ °C while hyperthermal ones are > 50 °C. The water samples were thus distributed in four groups. A first group, represented by low salinity samples comprises S1, D1, D2 and S2, with $0.3 \text{ g L}^{-1} \leq \text{TDS} \leq 0.92 \text{ g L}^{-1}$ and 12 °C $\leq T < 34$ °C. A second group, represented by brackish waters, includes samples D3-1, D3-2 and D3-3. The total dissolved solids content (TDS) and temperature ranged as follows $1.10 \text{ g L}^{-1} \leq \text{TDS} \leq 1.92 \text{ g L}^{-1}$ and 10.0 °C $\leq T \leq 21.5$ °C. A third group, with total dissolved solids comprised between $3.00 \text{ g L}^{-1} \leq \text{TDS} \leq 6.31 \text{ g L}^{-1}$, is composed of S3, S4, S5 and S6 samples, they are brackish waters. S3 and S6 samples with 27.0 °C $\leq T \leq 30.0$ °C are hypothermal waters while S4 and S5 are mesothermal waters with 39.5 °C $\leq T \leq 43.0$ °C. The fourth group is saline and hyperthermal water and concerns sample S7 with a $\text{TDS} = 17.25 \text{ g L}^{-1}$ and $T = 55$ °C. During the hydrochemical monitoring timespan (1993–2011), TDS and thus salinity increased in the waters of the two boreholes D1 and D2 by 162 and 178 mg L^{-1} respectively (Table 2). Nitrate levels reached 88 mg L^{-1} for D1. Being shallow this aquifer is then very sensitive to anthropogenic pollution, the standard guideline of WHO (2008) being 50 mg L^{-1} . The SO_4 concentration of D2 water increased during the monitoring period by 102 mg L^{-1} reaching 234 mg L^{-1}

Table 2 Physico-chemical parameters, major and minor elements and SiO₂ of groundwater in Mila's basin

Water point	Sampling date	T °C	pH	TDS mg·L ⁻¹	Ca ²⁺	Mg ²⁺	Na ⁺	K ⁺	HCO ₃ ⁻	Cl ⁻	SO ₄ ²⁻	NO ₃ ⁻	SiO ₂	Sr ²⁺	Li ⁺	Br ⁻
S1	03/02/2007	17.0	6.9	302	60	7	16	1	152	18	38	10				
D1	19/10/1993	21.0	7.9	452	80	12	32	1	122	65	102	38				
D1	02/07/2000	21.0	7.2	569	120	5	40	2	262	60	55	25	10.2			
D1	17/10/2000	20.0	7.3	615	110	19	38	1	220	90	82	55	7.9			
D1	08/04/2001	21.0	7.1	589	112	13	40	2	226	60	90	46	7.8			
D1	07/08/2001	20.0	7.3	555	31	55	50	1	232	70	54	62				
D1	13/01/2002	13.0	8.0	554	42	49	43	2	232	65	80	41				
D1	15/04/2004	20.0	7.6	592	72	43	22	2	207	50	140	56	8.5			
D1	12/11/2006	20.0	7.7	606	110	12	41	2	226	80	70	65				
D1	25/06/2007	22.0	7.3	605	104	15	37	2	189	60	136	62				
D1	17/05/2008	20.0	7.1	634	113	10	47	0	256	80	54	73	8.7			
D1	01/02/2009	12.0	7.2	683	124	16	44	2	256	85	68	88				
D1	16/03/2011	19.0	7.5	573	104	7	47	1	183	95	62	74				
D1	11/10/2011	19.0	7.3	614	101	12	50	2	201	95	80	72				
D2	24/01/1994	30.0	7.3	415	80	10	18	7	177	25	88	10				
D2	02/07/2000	30.0	7.3	611	120	17	22	2	250	20	164	16	11.2			
D2	08/04/2001	27.0	7.1	590	126	8	22	2	195	30	200	7				
D2	13/01/2002	27.0	7.7	583	42	71	24	2	177	42	224	1				
D2	07/04/2003	28.0	6.9	546	76	31	29	1	220	35	152	2				
D2	15/02/2004	30.0	7.8	594	72	53	14	2	256	30	162	5				
D2	12/11/2006	30.0	7.6	591	105	28	15	2	171	30	234	6				
D2	03/02/2007	29.0	7.5	583	105	28	13	3	232	35	160	7				
D2	17/05/2008	30.0	7.4	642	114	26	25	1	256	30	184	6	11.5			
D2	04/10/2009	28.0	7.2	628	107	24	34	2	238	40	178	5				
D2	11/10/2011	30.0	7.0	593	110	23	28	1	171	65	190	5				
D3-1	16/01/2000	16.0	6.9	1254	194	59	85	1	397	140	360	18	6.1			
D3-1	17/04/2000	18.0	7.0	1314	140	79	110	1	342	115	500	27	7.1			
D3-1	02/07/2000	20.0	7.1	1260	180	50	115	2	359	135	400	19	8.5			
D3-1	17/10/2000	21.0	7.0	1247	178	56	110	1	351	125	404	22	7.1			
D3-1	14/01/2001	17.0	7.6	1281	192	53	94	4	305	120	488	25	7.6			
D3-1	08/04/2001	16.0	6.9	1282	186	66	100	2	433	168	308	19	7.1			
D3-1	07/08/2001	21.5	7.0	1116	48	94	160	1	329	95	358	31				
D3-1	13/01/2002	13.0	7.8	1207	64	132	120	2	207	180	480	22				
D3-1	15/10/2002	10.0	7.9	1162	72	127	100	3	287	200	372	1				
D3-1	12/01/2003	20.0	7.5	1484	148	89	185	2	354	290	400	16				
D3-1	07/04/2003	19.0	6.7	1205	158	66	110	3	306	80	480	2				
D3-1	06/02/2005	12.0	7.0	1215	117	70	120	1	390	90	410	17				
D3-1	12/11/2006	21.0	7.5	1572	153	75	217	2	414	280	400	31	7.8			
D3-1	25/06/2007	21.5	7.4	1304	181	78	66	2	336	80	500	62				
D3-1	17/05/2008	20.0	7.3	1289	165	71	125	0	311	155	426	36	7.6			
D3-1	01/02/2009	13.0	6.9	1237	115	77	120	1	384	100	410	29				
D3-1	04/10/2009	21.0	7.1	1182	165	58	100	1	378	120	330	29				
D3-1	11/10/2011	20.0	7.0	1290	185	76	90	1	330	125	460	23				
D3-2	22/10/2010	21.5	6.9	1407	173	84	140	1	456	115	411	28				
D3-3	05/07/2013	20.5	7.0	1923	267	103	150	1	427	175	800	0				
S2	23/06/2012	33.0	7.2	923	128	24	130	1	220	215	200	5	14.0			
S2	01/10/2014	33.6	7.1	872	92	25	163	2	207	222	156	5	16.5	1.70	0.02	
S3	23/06/2012	27.0	6.8	3266	107	69	980	11	388	1166	545	0	16.0			

Table 2 continued

Water point	Sampling date	T °C	pH	TDS mg·L ⁻¹	Ca ²⁺	Mg ²⁺	Na ⁺	K ⁺	HCO ₃ ⁻	Cl ⁻	SO ₄ ²⁻	NO ₃ ⁻	SiO ₂	Sr ²⁺	Li ⁺	Br ⁻
S4	23/06/2012	39.5	6.3	2994	278	40	742	12	502	1178	242	0	28.0			0.96
S4	01/10/2014	39.7	6.4	3097	274	40	758	9	527	1224	227	0	23.1	7.17	0.37	0.96
S5	23/06/2012	43.0	6.3	3314	592	66	358	17	269	386	1626	0	32.0			0.01
S5	01/10/2014	41.9	6.5	3415	533	77	356	16	290	371	1673	0	29.2	13.23	0.37	0.01
S6	23/06/2012	30.0	6.8	6311	335	142	1560	7	415	1832	2020	0	21.0			
S6	01/10/2014	29.8	6.7	6648	363	172	1769	9	448	1788	2120	0	19.1	13.28	0.67	
S7	23/06/2012	55.0	6.0	17,252	1118	100	5602	94	758	8762	1109	0	74.0			2.50
S7	01/10/2014	56.6	5.8	17,543	1069	102	5459	87	709	8667	1159	0	62.1	34.05	4.32	2.50

which is just below the WHO guideline of 250 mg L⁻¹. Calcium contents of D1 and D2 exceed both the WHO standards of 100 mg L⁻¹. Silica content of the water from borehole D2 (11.5 mg L⁻¹) is higher than the 10 mg L⁻¹ standard line set by the WHO, knowing that this thermal borehole is used for drinking water supply. Sample S2 has a neutral water pH of 7.1, the hypothermal water is rich in chloride ions; its strontium content is 1.7 mg L⁻¹ and the Sr/Ca molar ratio = 8.45 ‰. The calculated carbon dioxide levels are comprised in the range: $0.13 \times 10^{-2} \leq P_{CO_2} \leq 2.6 \times 10^{-2}$ atm (Table 3) and are thus higher than CO₂ atmospheric pressure that equals 0.31×10^{-3} atm (Van der Weijden and Pacheco 2003). Saturation indices with respect to carbonate minerals: aragonite, calcite and dolomite (SI_a, SI_c and SI_d) are overall negative (Table 3). This could be related to fast and intensive infiltration (recharge) and very rapid drainage of newly infiltrated waters (Lopez-Chicano et al. 2001). It should be reminded that water is considered as undersaturated with respect to a given mineral when SI is < 0, it is in equilibrium with that mineral when SI = 0, whereas water is oversaturated when SI > 0 (Cidu et al. 2009). The saturation indices for evaporites: SI_{an} for anhydrite (CaSO₄), SI_g for gypsum (CaSO₄ · 2H₂O), SI_h for halite (NaCl) and SI_{sy} for sylvite (KCl) are negative and much lower than 0. The saturation indices for silicates: chrysotile, talc and sepiolite, (SI_{chr}, SI_t and SI_s) are found negative too. Regarding Group 2, the physico-chemical monitoring (2000–2011) of the waters from the detrital aquifer (D3-1) shows a large difference in temperature measured during pumping and at the surface (10 °C to 21.5 °C, Table 2). The pH values varied between 6.7 and 7.9. TDS has increased of 36 mg L⁻¹ during the survey period while the HCO₃ concentrations were found higher than 300 mg L⁻¹ which is a specific feature of carbogaseous waters (Grillot and Schoeller 1989). Water is

also rich in magnesium up to 132 mg L⁻¹ and sulphate ions with contents between 308 and 500 mg L⁻¹. These contents are much higher than those recommended by the WHO and set at 50 mg L⁻¹ for magnesium and 250 mg L⁻¹ for sulphates. Silica content is SiO₂ < 10 mg L⁻¹. The calculated groundwater P_{CO_2} reached 5×10^{-2} atm (Table 3) which is much higher than atmospheric P_{CO_2} . The hydrochemical composition of water from D3-2 borehole is similar to that of D3-1 one. However, D3-3 water exhibits a higher TDS. Saturation indices SI_{an}, SI_g and SI_h for all the analyzed water points are negative and much lower than 0 (Table 3). This means that groundwater is under-saturated with respect to the three afore-mentioned minerals. SI_c saturation indices are found positive for the majority of samples. Saturation indices for silicates (SI_{cha}, SI_{chr}, SI_t and SI_s) are found negative. Regarding the third group, its waters are slightly acidic waters $6.3 \leq \text{pH} \leq 6.8$. Three subgroups can be distinguished, waters that are rich in chlorides and relatively poor in SO₄, samples S3 and S4, respectively Cl = 1166 and 1178 mg·L⁻¹ and SO₄ = 545 and 242 mg L⁻¹. The presence of a smell of rotten eggs was noted in S4 revealing the presence of hydrogen sulphide gas (H₂S). A subgroup, sample S5, with a Cl concentration of 385.7 mg L⁻¹ and a high SO₄ content reaching 1626.2 mg L⁻¹. A subgroup, sample S6, rich in Cl = 1832 mg L⁻¹ and in SO₄ = 2020 mg L⁻¹. The waters of S5 and S6 have the same strontium concentration (13.2 mg L⁻¹) that is higher than what was recorded for S4 (7.17 mg L⁻¹). The Sr/Ca molar ratios of S4, S5 and S6 are successively of 11.94‰, 9.55‰ and 16.72‰ which are considered as very high. The water of S4 is richer in bromide ion than that of S5 with respectively 0.96 mg L⁻¹ and 0.01 mg L⁻¹. P_{CO_2} is high and reached 26.3×10^{-2} atm in sample S4 and the SI_c, SI_d and SI_a are found negative. The saturation indices in evaporate

Table 3 P_{CO_2} , Mg/Ca ratio and saturation indices for the main minerals

Ref	Sampling Date dd/mm/yyyy	P_{CO_2} atm $\times 10^{-2}$	Mg/Ca ratio	Saturation indices															
				Aragonite	Calcite	Dolomite	Anhydrite	Gypsum	Halite	Sylvite	Chalcedony	Chrysotile	Talc	Quartz	Sepiolite	SiO ₂ (a)			
S1	03/02/2007	1.659	0.19	-0.85	-0.70	-2.10	-2.40	-2.01	-8.10	-8.83									
D1	19/10/1993	0.134	0.24	0.18	0.33	0.13	-1.89	-1.55	-7.25	-8.31									
D1	02/07/2000	1.445	0.06	-0.01	0.14	-0.81	-2.02	-1.67	-7.19	-8.05	-0.17	-8.96	-5.43	0.27	-6.17	-1.02			
D1	17/10/2000	0.954	0.28	-0.05	0.09	-0.29	-1.92	-1.56	-7.04	-8.17	-0.27	-6.78	-8.17	0.17	-5.00	-1.13			
D1	08/04/2001	1.584	0.19	-0.22	-0.07	-0.78	-1.85	-1.50	-7.19	-8.05	-0.29	-8.35	-5.28	0.15	-6.11	-1.14			
D1	07/08/2001	1.023	2.92	-0.56	-0.42	-0.30	-2.63	-2.27	-7.00	-8.20									
D1	13/01/2002	0.181	1.92	0.14	0.30	0.83	-2.39	-1.95	-7.12	-7.97									
D1	15/04/2004	0.446	0.98	0.02	0.17	0.39	-1.88	-1.52	-7.53	-8.13									
D1	12/11/2006	0.389	0.17	0.36	0.51	0.34	-1.97	-1.61	-7.06	-7.92									
D1	25/06/2007	0.851	0.23	-0.12	0.02	-0.49	-1.70	-1.36	-7.24	-8.02	-0.23	-8.70	-5.50	0.22	-8.19	-1.08			
D1	17/05/2008	1.778	0.14	-0.17	-0.02	-0.81	-2.07	-1.71	-7.00	-7.85									
D1	01/02/2009	1.258	0.21	-0.16	-0.01	-0.75	-2.03	-1.58	-7.00	-7.85									
D1	16/03/2011	0.501	0.11	0.04	0.19	-0.52	-2.04	-1.67	-6.92	-8.14									
D1	11/10/2011	0.870	0.19	-0.14	0.01	-0.64	-1.96	-1.59	-6.90	-7.84									
D2	24/01/1994	0.891	0.20	-0.09	0.05	-0.40	-2.38	-2.13	-7.37	-7.37									
D2	02/07/2000	1.230	0.23	0.16	0.30	0.14	-1.50	-1.25	-7.94	-8.58	-0.24	-5.49	-2.20	0.18	-4.45	-1.06			
D2	08/04/2001	1.479	0.10	-0.17	-0.03	-0.90	-1.42	-1.14	-7.76	-8.39									
D2	13/01/2002	0.331	2.78	-0.10	0.04	0.66	-1.89	-1.6	-7.58	-8.54									
D2	07/04/2003	2.691	0.67	-0.50	-0.36	-0.74	-1.73	-1.46	-7.57	-8.62									
D2	15/02/2004	0.630	1.21	0.24	0.38	1.03	-1.75	-1.50	-7.96	-8.4									
D2	12/11/2006	0.371	0.44	0.17	0.31	0.43	-1.42	-1.17	-7.94	-8.4									
D2	03/02/2007	0.741	0.43	0.30	0.44	0.71	-1.55	-1.33	-7.94	-8.17									
D2	17/05/2008	1.000	0.37	0.24	0.38	0.50	-1.50	-1.25	-7.71	-8.70	-0.22	-4.35	-1.03	0.19	-6.69	-1.05			
D2	04/10/2009	1.445	0.36	-0.04	0.10	-0.08	-1.54	-1.27	-7.45	-8.27									
D2	11/10/2011	1.698	0.34	-0.34	-0.20	-0.70	-1.48	-1.23	-7.33	-8.37									
D3-1	16/01/2000	3.890	0.50	-1.14	0.01	-0.27	-1.26	-0.86	-6.53	-8.00									
D3-1	17/04/2000	2.344	0.93	-0.24	-0.09	-0.17	-1.21	-0.88	-6.51	-8.10	-0.29	-7.01	-4.42	0.16	-5.40	-1.10			
D3-1	02/07/2000	2.754	0.45	0.04	0.19	0.10	-1.26	-0.85	-6.42	-7.73	-0.24	-7.45	-3.85	0.21	-5.09	-1.18			
D3-1	17/10/2000	2.951	0.51	-0.06	0.09	-0.04	-1.20	-0.86	-6.48	-8.07	-0.33	-7.49	-1.36	0.21	-5.6	-1.12			
D3-1	14/01/2001	0.602	0.45	0.44	0.58	0.84	-1.14	-0.75	-6.56	-7.47	-0.26	-4.44	-1.36	0.12	-3.29	-1.15			
D3-1	08/04/2001	4.265	0.58	-0.11	0.04	-0.16	-1.35	-0.95	-6.39	-7.62	-0.25	-8.45	-5.4	0.20	-5.94	-1.13			
D3-1	07/08/2001	2.818	3.22	-0.63	-0.49	-0.40	-1.79	-1.44	-6.43	-8.19									
D3-1	13/01/2002	0.245	3.40	-0.07	0.08	0.65	-1.66	-1.22	-6.27	-7.57									
D3-1	15/10/2002	0.257	2.90	0.19	0.34	1.05	-1.73	-1.26	-6.30	-7.33									
D3-1	12/01/2003	0.912	0.99	0.33	0.48	1.01	-1.34	-0.98	-5.89	-7.41									
D3-1	07/04/2003	0.68	-0.51	-0.36	-0.84	-1.20	-0.84	-6.67	-7.78										

minerals (SI_{an} , SI_g , SI_h) and the saturation indices for celestite ($SrSO_4$) and strontianite ($SrCO_3$) are negative for all these brackish waters except for spring S5 with $SI_{celestite} = 0.06$. All the waters in this group are rich in SiO_2 , with the highest contents in the S5 sample of 32 mg L^{-1} . The fourth group, represented by sample S7 which pH is acidic (5.95); the levels of the analyzed major ions are high, chlorides reach 8762 mg L^{-1} and sodium 5602 mg L^{-1} . The presence of a sulphurous smell is noted. It is one of the most saline thermal springs in Algeria (Dib 2008). Strontium content is 34 mg L^{-1} and that of Lithium 4.32 mg L^{-1} , whereas the Sr/Ca molar ratio is high as it reaches 13.92%. The bromide content is 2.5 mg L^{-1} . The calculated $P_{CO_2} = 128.8 \times 10^{-2} \text{ atm}$ (in 2014) and $83.17 \times 10^{-2} \text{ atm}$ (in 2012) are extremely high. The saturation indices of the evaporite minerals SI_{an} , SI_g , SI_h , SI_{sy} and $SI_{celestite}$ (Table 3) and those of the silicates (IS_{chr} , SI_s , SI_s), are all negative confirming the dissolution of the considered minerals. On the surface, near the S6 and S7 springs, and along the Maleh wadi, we note the presence of mineral precipitation (saline in taste) probably due to evaporation ($ETP = 1151 \text{ mm y}^{-1}$) of these waters.

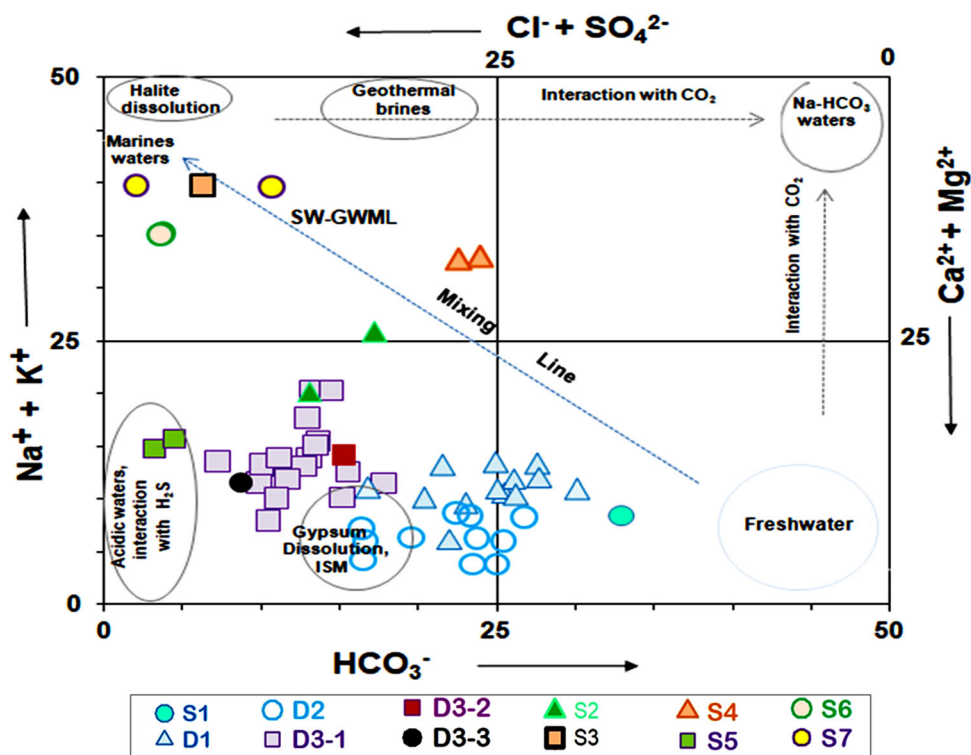
The Piper’s classification and Langelier–Ludwig diagram (Fig. 2) show that the freshwaters of the first group S1 and D1 have a HCO_3 –Ca hydro-facies. The waters of D2 are richer in sulphates and evolve from the HCO_3 –Ca type to the SO_4 –Ca one. S2 spring has an overall Cl – SO_4 –Ca facies. All samples of the second group of waters (D3-1,

D3-2 and D3-3) are of the SO_4 –Ca–Mg type. The third group are Cl –Na waters, except for spring S5 water which is SO_4 –Ca. The fourth group (S7) exhibits a hyperchloride–sodium hydrofacies.

3.1 Mineralisation processes and origin of the main dissolved ions

The molar ratios HCO_3/Na vs. Ca/Na and Mg/Na versus Ca/Na (Fig. 3a, b) are widely used to elucidate the sources of dissolved major ions (Gaillard et al. 1999). The graphs of Fig. 3a, b show the evaporitic and silicate geochemical signatures of the waters. In order to determine the nature of the ions in solution, the processes of salinity acquisition and the possible mixings between waters from different lithologies, the correlations between the major ion contents and the molar ratios were studied. According to the Langelier–Ludwig diagram (Fig. 2), the waters are globally distributed in a triangle with three very different chemical end-members namely calcium–bicarbonate water, hyperchloride–sodium water and a calcium–sulphate cluster at the water boundary where the presence of hydrogen sulphide is observed. On the binary diagram of Fig. 3c, Na^+ versus Cl^- , the SeaWater Mixing Line (SWML) (Quinby-Hunt and Turehian 1983), and the Halite Dissolution Line (HDL) are reported. The correlation shows: the dissolution of Halite $NaCl \rightarrow Na^+ + Cl^-$ (Process 1) on one hand and on the other hand a mixing between an end of recharge

Fig. 2 Langelier–Ludwig diagram illustrating the mixing between the three main types of water. (SW–GWML, Seawater Groundwater Mixing Line; ISM, Interaction with Sulphate Minerals)



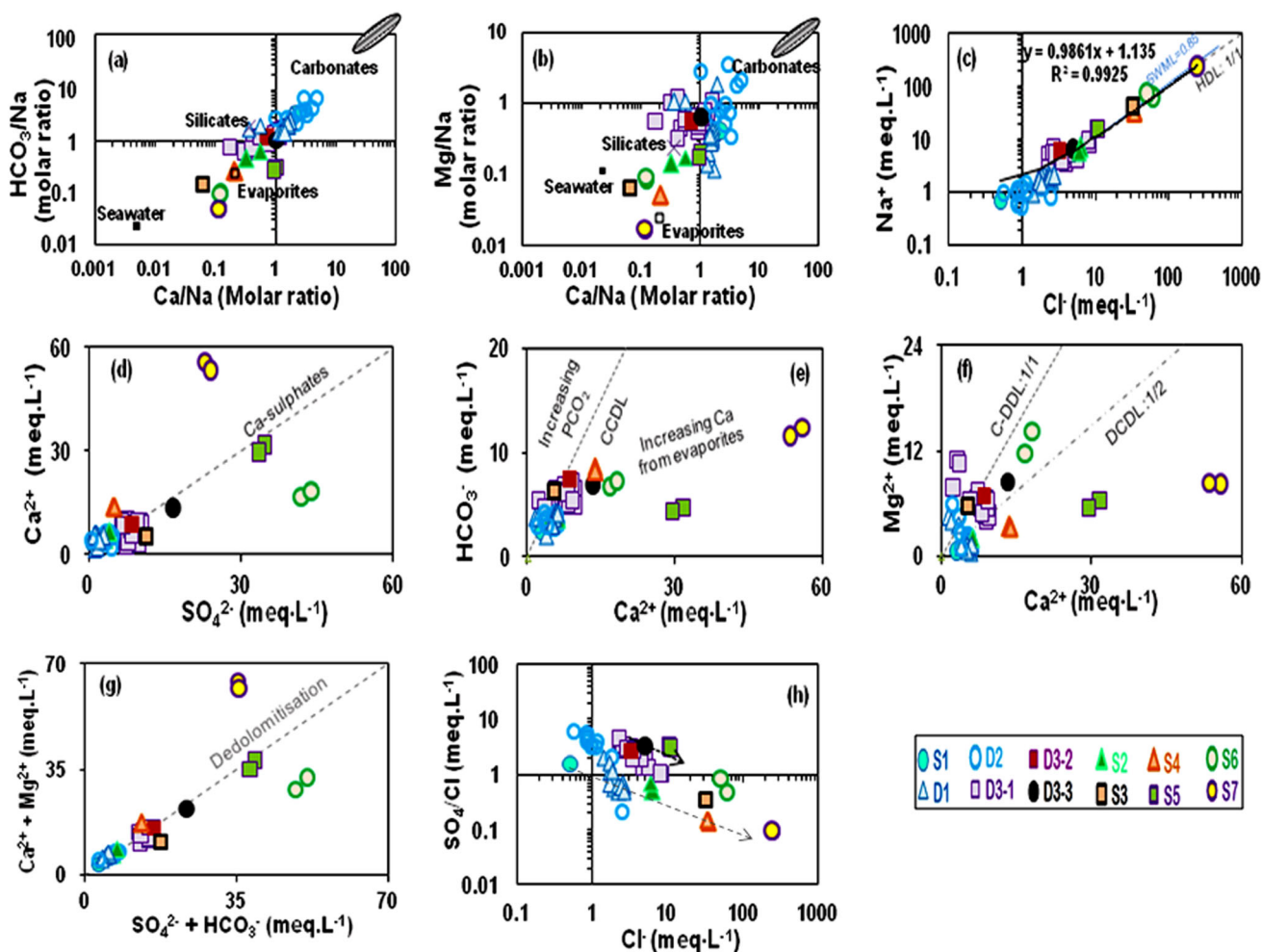


Fig. 3 a, b HCO_3^-/Na versus Ca/Na ratio and Mg/Na versus Ca/Na ratio; c Na^+ versus Cl^- , (HDL, Halite Dissolution Line; SWML is the current Seawater Mixing Line); d Ca^{2+} versus SO_4^{2-} , (GDL, Gypsum Dissolution line); e HCO_3^- versus Ca^{2+} , (CCDL, Calcite Congruent Dissolution Line); f Mg^{2+} versus Ca^{2+} , (DCDL, Dolomite Congruent Dissolution Line, CDDL: Calcite–Dolomite Dissolution Line); g $\text{Ca}^{2+} + \text{Mg}^{2+}$ versus $\text{SO}_4^{2-} + \text{HCO}_3^-$; h SO_4/Cl ratios versus Cl^-

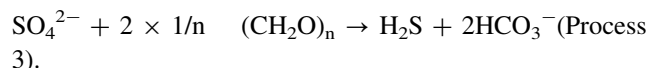
water (freshwater S1) and salt-water which corresponds in the present case to thermal waters of S7. $\text{Na}/\text{Cl} > 1$ can be associated with water–rock interaction involving other sodium minerals.

Ca^{2+} versus SO_4^{2-} plot (Fig. 3d) shows dissolution of sulphate salts: (Process 2).

According to Bishop et al. (2014) gypsum and anhydrite are the most commonly occurring Ca–Sulphates minerals on the earth together with Bassanite ($\text{CaSO}_4 \cdot 0.5 \text{H}_2\text{O}$).

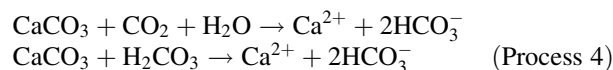
[(gypsum $\text{CaSO}_4 \cdot 2\text{H}_2\text{O} \rightarrow \text{Ca}^{2+} + \text{SO}_4^{2-} + \text{H}_2\text{O}$ and/or anhydrite: $\text{CaSO}_4 \rightarrow \text{Ca}^{2+} + \text{SO}_4^{2-}$).

The low SO_4^{2-} content of S4 and S7 is due to the phenomenon of sulphate reduction by bacteria (Appelo and Postma 2005); the smell of sulphur is characteristic at these water points. Generally, this process occurs in a closed environment as the consequence of anaerobic reducing conditions. The process of sulphate reduction is as follows:

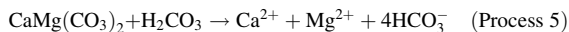


HCO_3^- versus Ca^{2+} (Fig. 3e) and Mg/Ca ratios < 0.5 (Table 2) show congruent dissolution of calcite with the exception of two samples from D3-1 which show incongruent dissolution of dolomite confirmed by the Mg^{2+} versus Ca^{2+} correlation (Fig. 3f). Indeed, the significant increase in the $\text{Mg}/\text{Ca} > 2$ ratio, the positive IS_c and IS_d (Table 3) and the decrease in HCO_3^- concentrations confirm the incongruent dissolution of dolomite (Fairchild et al. 2000). This explains the depletion in Ca^{2+} in comparison with SO_4^{2-} and Mg^{2+} contents.

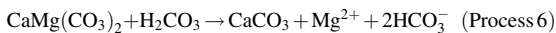
– Congruent Dissolution of Calcite



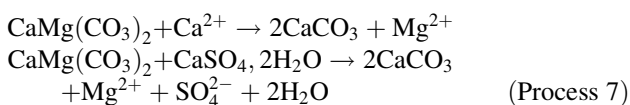
– Congruent Dissolution of Dolomite



– Incongruent Dissolution of Dolomite



The Mg/Ca ratio = 3.22 of sample D3-1 during the low waters' period in August 2001 (Table 3) shows an IS_c and $\text{IS}_d < 0$, the increase in temperature ($T = 21.5^\circ\text{C}$) and $P_{\text{CO}_2} = 2.8 \times 10^{-2}$ atm, confirm an upward inflow of thermal water. Karst thermal water S2, (sample 2012), with positive IS_c and IS_d and a $P_{\text{CO}_2} = 1.41 \times 10^{-2}$ atm, indicates that the water is flowing in an aerated environment probably an open conduit. Karst thermal water of D2 with positive IS_c and IS_d and a $P_{\text{CO}_2} = 0.3 \times 10^{-2}$ atm means that groundwater circulates in an aerated environment, that is enriched in CO_2 of atmospheric origin. The correlation $\text{Ca}^{2+} + \text{Mg}^{2+}$ versus $\text{SO}_4^{2-} + \text{HCO}_3^-$ (Fig. 3g) shows that for spring S5, water undergoes a dedolomitization process that converts dolomite into calcite (Schoenherr et al. 2018):



This is not the case for S6 and S7 because of the high chloride contained in their waters. The aforementioned process is an evidence of the existence of strong hydrothermal alteration.

The SO_4/Cl versus Cl diagram (Fig. 3h) could be used as an indicator of sulphate sources in groundwater (Farid et al. 2015). The plot illustrated by Fig. 3h indicates the presence of two types of mixing. The first one occurs in the Cretaceous karst aquifer where a fresh recharge component (S1 with $\text{SO}_4/\text{Cl} = 1.54$) intermingles with a more mineralised thermal component represented by S4 with a mean $\text{SO}_4/\text{Cl} = 0.14$. All D2 samples have $\text{SO}_4/\text{Cl} > 2$ reflecting thus intensive dissolution of sulphate minerals. The second mixing occurs in Group 2 aquifer with $\text{SO}_4/\text{Cl} = 4.6$ (D3-1) and an increase in temperature which reaches 21.5°C (June-2007) (Table 2). This indicates a contribution from a hot sulphate-rich water component. Sample from D3-1 exhibit a $\text{SO}_4/\text{Cl} = 3.6$ during high-water periods (2005) ($T = 12^\circ\text{C}$) meaning that sulphates are also of superficial origin through the dissolution of Mio-Pliocene gypsum (Vila 1980; Coiffet 1992) and fed by the Boussellah wadi inflow. Thermal waters of S4 and S7 waterpoints show low SO_4/Cl ratios of 0.15 and 0.09 respectively. This is attributed to a reduction of sulphates. The Sr/Ca molar concentration ratios for all the thermal springs are comprised between 8.4 and 16%. According to Meybeck (1984) in Hsissou et al. (1996), Sr/Ca molar ratios higher

than 1‰ are typical of evaporitic waters and are due to the dissolution of celestite (SrSO_4) and strontianite (SrCO_3) (Process 8). The dissolution of these minerals is confirmed by the negative saturation indices of celestite and strontianite (Table 3). Lithium content of spring S7 equals 4.32 mg L^{-1} , it is the highest value obtained among all the analyzed spring waters. It is most probably due to a water's high temperature, since a small increase in temperature is sufficient enough to cause an increase in the groundwater Li^+ content by 100 to 10,000 times (Barbieri et al. 1998 in, El Achheb et al. 2003).

It is also noted that the silicates brought into solution are in fact magnesian silicate minerals, namely Talc [$\text{Mg}_3\text{Si}_4\text{O}_{10}(\text{OH})_2$], Chrysotile [$\text{Mg}_3\text{Si}_2\text{O}_5(\text{OH})_4$], and Sepiolite [$\text{Mg}_4\text{Si}_6\text{O}_{15}(\text{OH})_2 \cdot 6\text{H}_2\text{O}$]. The saturation indices for those minerals are negative for all samples. (Process 9).

In order to determine the origin of the chlorides, the average Br/Cl ratio of seawater ($1.52 \pm 0.01 \times 10^{-3}$) (Quinby-Hunt and Turehian 1983), and that of halite (0.1×10^{-3}) (Fontes and Matray 1993) are plotted against the Cl^- concentrations (Alcalá and Custodio 2008) (Fig. 4). Thermal waters S4, S5 and S7 are found very close to the right side of the Br/Cl ratio of halite.

3.2 Depth of the geothermal reservoir

Giggenbach (1988) Na–K–Mg diagram Fig. 5a allows one to distinguish between the different water masses of the deep reservoirs: those in full equilibrium from those in partial equilibrium from those that are immature. Only the waters of S7 spring are in partial equilibrium, the waters of S6, S5 and S4 are at the borderline between the immature ones and those with partial equilibrium. Waters from the points S1, S2, D1, D2, D3-1, D3-2 fall all within the domain of immature waters. Giggenbach (1991) $\text{Cl}-\text{SO}_4-\text{HCO}_3$ ternary diagram Fig. 5b shows that water from the S5 spring is very close to the volcanic waters' domain, the

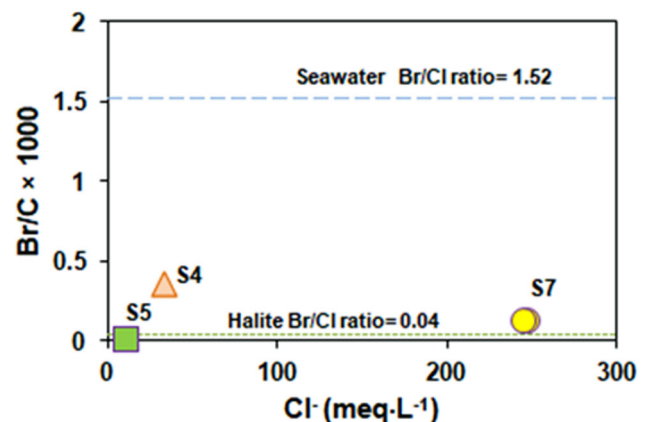


Fig. 4 Correlation between Br/Cl molar ratio and Cl^- content

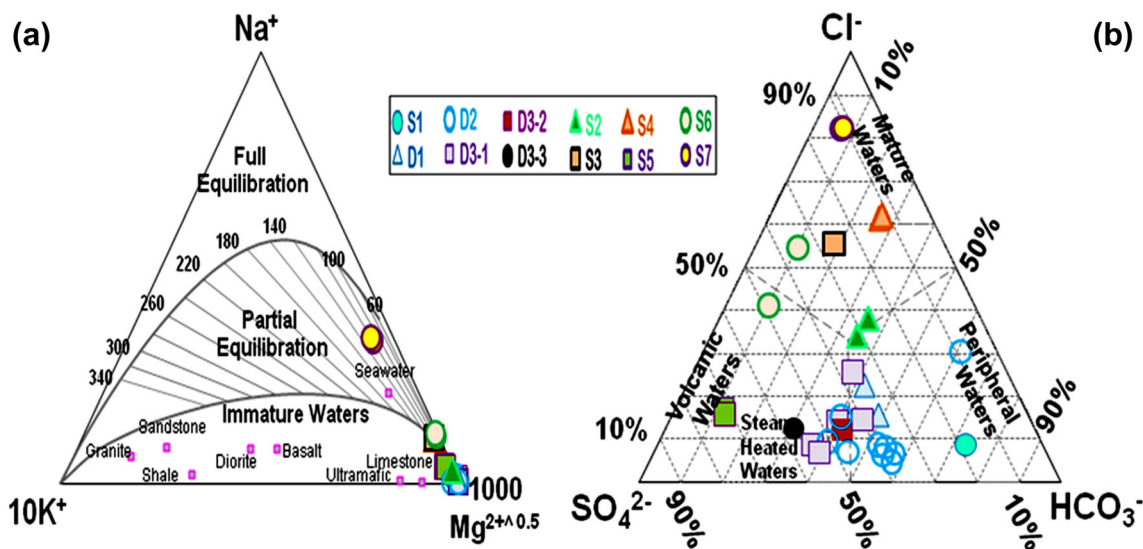


Fig. 5 a Ternary diagram Na–K–Mg according to the model of Giggenbach (1988); b Ternary diagram Cl–SO₄–HCO₃ according to the model of Giggenbach (1991)

water from sample D3-3 is in the steam heated waters domain, the water from sample D2 which is in the peripheral waters' domain corresponds to the sample taken in January 1994 at the beginning of pumping. Overall, this diagram shows mixtures between recharge waters (bicarbonate), evolved hyperchloride waters and sulphate waters that are influenced by magmatic fluids (most probably steam). The depth of the geothermal reservoirs was obtained by calculating the temperature of the thermal fluid through conventional geothermometers (Table 4) and by applying the regional geothermal gradient estimated by (Kedaid 2007; Chenaker et al. 2018) i.e. 3.85 °C/100 m for the Mila basin. The results in Table 4 show that S7 spring reservoir is the hottest, with temperatures ranging between 116.06 and 119.93 °C, indicating a reservoir depth comprised between 3104.7 and 3115 m. These temperatures are the averages of the results computed by means of the silica and the cationic geothermometers for the two periods 2012 and 2014. The deepest compartment would be the S5 spring, which could be as deep as 3787.9 m (as estimated by the cationic geothermometers) while silica geothermometers give a depth of 2121.6 m.

The thermal water compartments D2, S2, S3, S4 and S6 would be between 1218 and 2828.3 m deep. The large discrepancy between the temperatures estimated by the classical cationic and silica geothermometers (Table 4), led us to complete our investigation on the depth of the thermal reservoir, by comparing the calculated saturation indices of the different minerals in the water, (used as geothermometer) (Mutlu and Güleç 1998; Saibi et al. 2021) (Fig. 6). The temperature modelling performed by means of a geochemical software package (Phreeqci-3.1.4-8929) developed by Parkhurst and Appelo (2013) was applied to

all the studied thermal waters. The investigations were conducted at different temperatures (30–180 °C). The calculations of the water–mineral equilibria are shown in Fig. 6.

All waters at different temperatures are undersaturated in Halite, Gypsum, Sylvite, Sepiolite, Strontianite and Silica (amorphous), the water of S5 spring shows an $IS_g > 0$ for a temperature of 90 °C. Only IS_{talc} and $IS_{\text{chrysolite}}$ indicate that equilibrium is reached at high temperatures; the thermal fluid that comes in contact with the magnesian silicates is undersaturated towards these minerals (water–rock interaction with magnesian silicates). Overall, the modelled “water–mineral” equilibria give temperatures close to those of the silica geothermometers.

3.3 Conceptual model

Based on all the results discussed in the previous paragraphs and on the geological setting of the region of interest, we made a trial in developing a conceptual model (Fig. 7) that aims at explaining the water salinization processes as well as how the hydrothermal circulation takes place in Mila's basin.

There are two main geothermal reservoirs:

- (i) a brackish thermal water reservoir whose waters interact with a geothermal fluid of volcanic origin. The geochemical signature of the water at emergence (S5) shows contact with Triassic formations that are rich in Ca-sulphates in addition to the alteration of magnesian silicates. The geothermal water flows through Cretaceous carbonate formations via faults in the Redjas collapse ditch.

Table 4 Estimation of the temperature of the thermal reservoir using cationic and silica geothermometers

Ref	Sampling year	(A) Na–K–Ca geothermo-meter T (°C)	(B) Na–K geothermometers	(C)	Average Temperature geothermo-meters	Cationic Silica geothermometers	(D)	(E)	(F)	(H)	Average temperature
D2	2008	71.36	168.16	149.02	129.51		43.85	51.41	42.56	49.74	46.89
S2	2012	104.30	86.56	65.19	85.35		50.54	57.44	49.80	55.80	53.39
S2	2014	109.22	116.38	95.48	107.02		56.49	62.76	56.10	61.15	59.12
S3	2012	132.67	102.54	81.36	105.52		55.25	61.65	54.80	60.04	57.93
S4	2012	122.04	119.36	98.54	113.31		76.58	80.56	76.71	79.08	78.23
S4	2014	122.42	106.05	84.94	104.47		68.88	73.77	68.90	72.23	70.94
S5	2012	107.43	177.52	158.82	147.92		82.08	85.40	82.24	83.95	83.41
S5	2014	106.90	172.16	152.21	143.75		78.42	82.18	78.56	80.71	79.96
S6	2012	131.15	66.03	44.51	80.58		65.28	70.58	65.22	69.03	67.52
S6	2014	132.21	71.28	49.78	84.42		61.70	67.40	61.53	65.82	64.11
S7	2012	141.04	118.66	97.81	119.17		121.03	119.04	121.43	117.89	119.84
S7	2014	141.09	120.91	100.12	120.7		112.24	111.52	112.45	112.98	112.29

(A) Fournier & Truesdell 1973:

$$T^{\circ}\text{C} = [1647/(\text{Log}(\frac{\text{Na}}{\text{K}}) + \beta \cdot (\text{Log}\sqrt{\text{Ca}/\text{Na}} + 2.24))] - 273.15 \text{ with } \beta = 4/3 \text{ for } T < 100^{\circ}\text{C}, \beta = 1/3 \text{ for } T > 100^{\circ}\text{C}$$

(B) Nieva and Nieva 1987: $T^{\circ}\text{C} = [1390/(\text{Log}(\text{Na}/\text{K}) + 1.750)] - 273.15$

(C) Giggenbach 1988: $T^{\circ}\text{C} = [1217/(\text{Log}(\text{Na}/\text{K}) + 1.483)] - 273.1$

(D) Fournier 1977: $T^{\circ}\text{C} = [1309/(5.19 - \text{Log}(\text{SiO}_2))] - 273.15$. Quartz, no steam loss (conductive)

(E) Fournier 1977: $T^{\circ}\text{C} = [1522/(5.75 - \text{LogSiO}_2)] - 273.15$. Quartz, maximum steam loss at 100 °C (adiabatic)

(F) Fournier & Potter 1979: $T^{\circ}\text{C} = -42.2 + 0.28831S - 3.6686 \times 10^{-4}S^2 + 3,1665 \times 10^{-7}S^3 + 77.034 \cdot \log S$ Quartz (25–900 °C)

(G) Arnórsson et al. 1983: $T^{\circ}\text{C} = [1498/(5.70 - \text{Log}(\text{SiO}_2))] - 273.15$

NB. All the calculations are made using the mg L⁻¹ as a unit for the concentrations of the cations and silica

At the lateral extremities of the basin, geothermal fluids of volcanic origin contaminate the Mio-Plio-Quaternary aquifer in the Ferdjioua ditch (D3-1, D3-2, D3-3) to the west, where the water is brackish and carbonated. To the east of the basin, the geothermal fluids are less perceptible at Jebel Lakhhal (D2), mainly due to the mixing with infiltrating rainfall water. Borehole water surveyed in the framework of the present study is all intended for drinking water supply.

- (ii) a geothermal reservoir whose water of the hyperchloride chemical facies flows through NaCl-rich Triassic formations (Halite). This reservoir has also a magnesian silicate component. It is thought to be the source of two sub-reservoirs namely an oxygen-poor water compartment (S4) and a shallower water compartment that is diluted by an infiltrating precipitation water component (S2).

A mixture of water from the two main geothermal reservoirs (S6 and S3) discharges into Maleh wadi. The latter most probably originates from a deep tectonic fault. It

should be noted that this wadi allows surface water to infiltrate during high-water periods.

4 Conclusions

An increase in groundwater salinity in the aquifer complex of the study area recorded over a decade of hydrochemical monitoring was observed. An attempt was made in order to decipher and characterise the origin of the dissolved salts and the different hydrogeochemical processes controlling the salinization of water. The increase in TDS in the detrital aquifer of the graben has two origins. It is due to: (i) the infiltration of water from the Boussellah wadi (superficial soil's leaching) during humid periods and (ii) an upwelling and a mixing with saline and hot water of deeper origin. The brackish and carbogaseous groundwater used for drinking water allocation exhibits Ca²⁺, Mg²⁺ and SO₄²⁻ contents that exceed the guideline values recommended by the WHO (2008). The shallow karstic aquifer tapped by borehole D1 is a highly fractured aerated horst. It is fed by rapid infiltration of precipitation through the thin

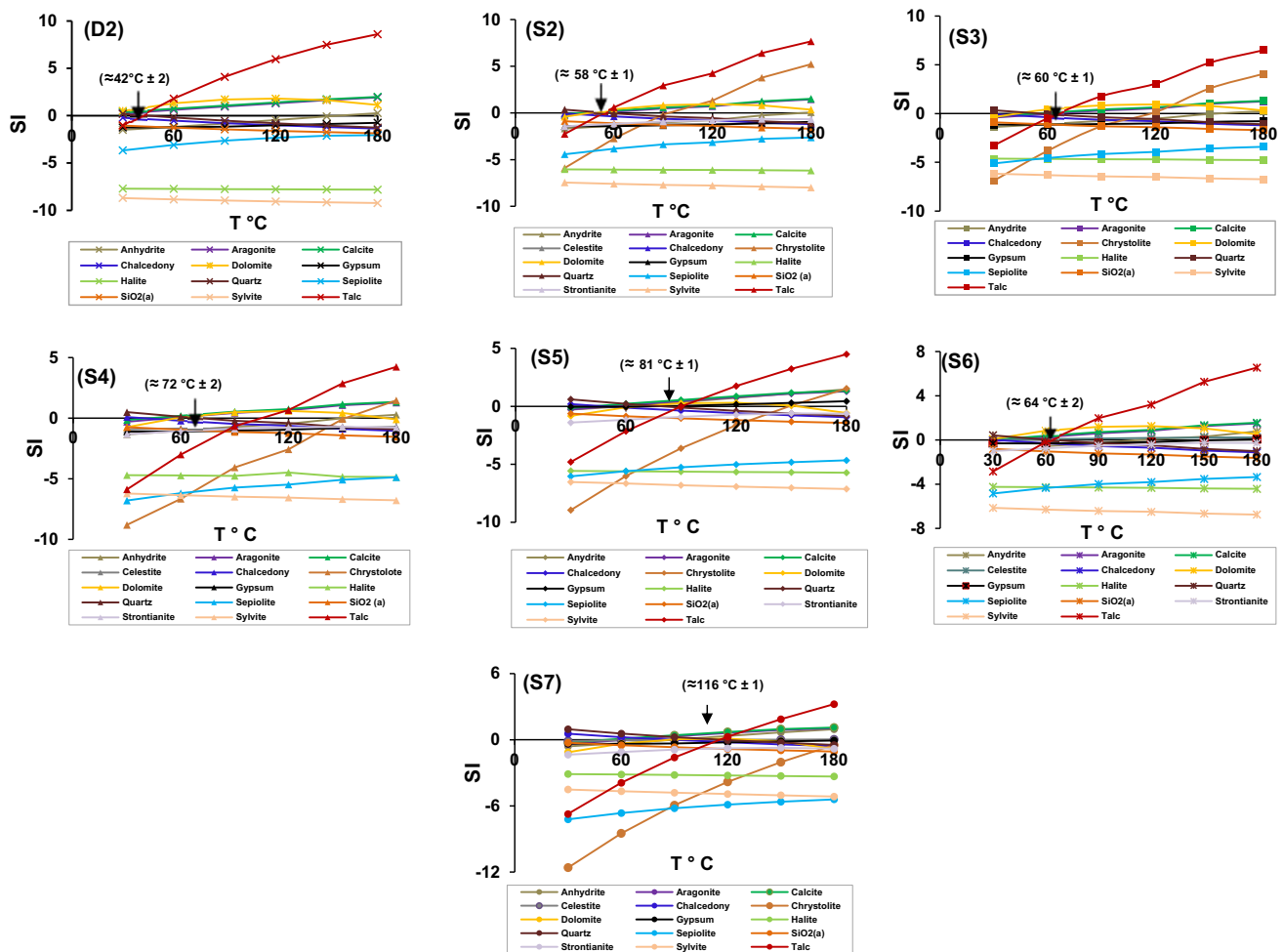


Fig. 6 Mineral equilibrium diagrams for sampled thermal waters from Mila's basin

superficial formations that lie on it. It is thought to be related to the thermal aquifer with CO₂-rich fluid inputs under specific circumstances of excessive pumping and dry periods which explains the increased TDS. This karst aquifer is contaminated by nitrates and the levels exceed WHO standards (WHO 2008). The thermal karst tapped by borehole D2 exhibits an increase in TDS of 178 mg L⁻¹ after 17 years of pumping. It suffered from an increase of 102 mg L⁻¹ in sulphates which would originate from a dissolution of evaporites and/or mixing with water of deep origin that is loaded with SO₄. Water circulates in an aerated karstic environment in the vicinity of the spring. This aquifer has SiO₂ contents that exceed the WHO guidelines for water consumption. The geothermometry and hydrogeochemistry of groundwater show that all thermal waters are in contact with Triassic evaporite minerals. They are all immature waters except for S7 spring which is partially in equilibrium. The latter is thought to sit at a depth ranging between 3014.7 and 3115 m and is the hottest reservoir in the Mila basin

(T ≈ 116 °C). The waters of S5 spring would be in contact with gaseous fluids of magmatic origin that happen to be rich in H₂S at a depth comprised between 2121.6 and 3788 m. Isotopic analyses of SO₄ would allow their origin to be more accurately determined. The thermal waters from D2, S2, S3, S4 and S6 are mixtures of evolved hyperchloride-sodium water, sulphated water and bicarbonate recharge water. The karstic thermal waters from D2 and S2, lie respectively on average between 1280 and 3363 m, 1461 and 2760 m deep. They are more affected by recharge waters and therefore get more diluted. The thermal waters from S3 and S6 are mixed with infiltrating water containing dissolved salts, from the Maleh wadi at an average depth ranges of respectively 1504.6 to 2740 m, and 1709.6 to 2143 m. The thermal waters of S4 occur in a reducing environment and contain CO₂ indicating a closed environment at an average depth interval of 1937.4–2828.4 m. Deep waters, with a strong hydrothermal alteration ascend through faults and fractures contributing to the contamination of shallower aquifers used

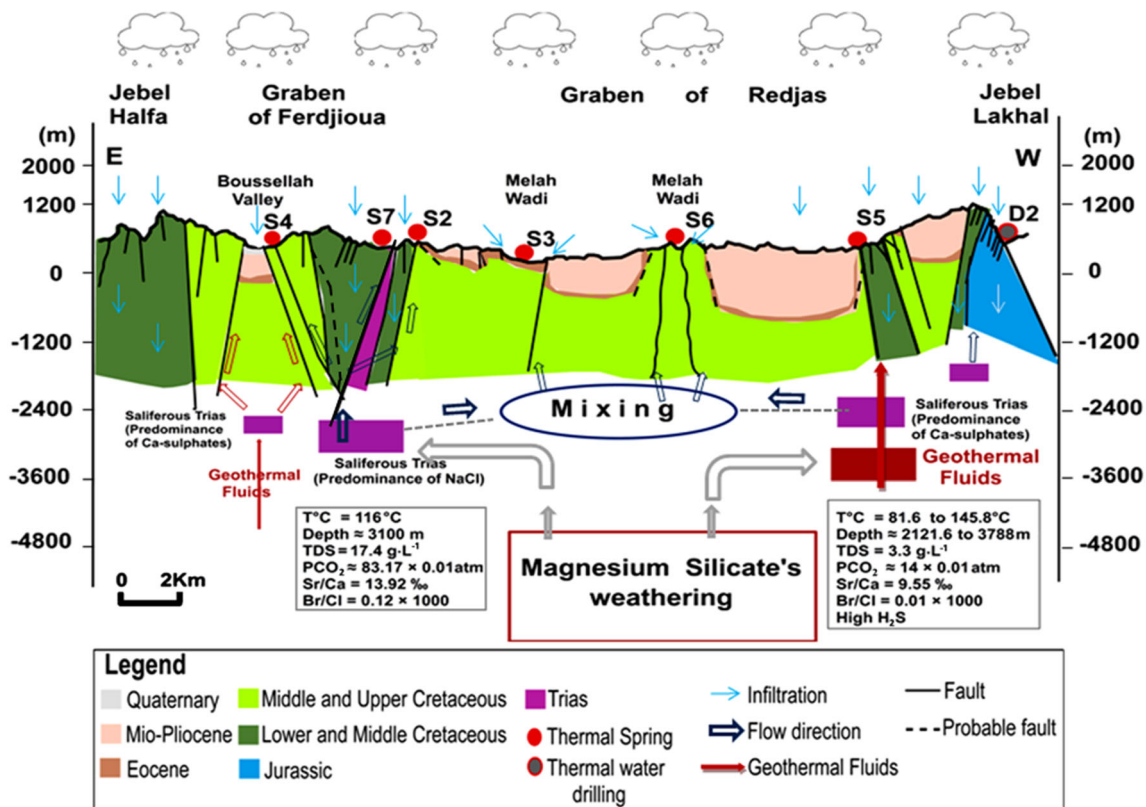


Fig. 7 Conceptual model reflecting mineralization acquisition and groundwater circulation

for drinking water supply. A conceptual model explaining the functioning of the hydrothermal complex of the Mila basin is proposed.

Author contributions The study conception and design were performed by the first author YBO who carried out the collection and the treatment of the whole dataset. The remaining of the co-authors contributed each one in their field of competency to the production of the paper as follows: YBO & ASM in data processing, interpretation and drafting of the document; AK contributed in gathering the geological data and provided his expertise in locating the faulting network. The first draft of the manuscript was written by YBO & ASM. All three authors commented on previous versions of the manuscript. The final manuscript was reviewed and endorsed by the three authors.

Data availability The authors declare that there exist no confidentiality constraints on the availability of all the data that were used in the present study. All the information collected on site or generated by the laboratory analyses throughout the course of this investigation are included in this article.

Declarations

Conflict of interest The authors have no relevant financial or non-financial interests to disclose with regard to the work described in the present paper. The authors declare that they received no financial aid, neither in the form of grants nor any other kind of specific funds to support the present investigation during its whole course.

References

- ABH (2004) The watershed of the Kebir-Rhumel. Constantinois-Seybouse-Mellegue Hydrographic Basin Agency. The Notebooks of the Agency no. 8: 1–44.
- ADE Mila (2013) Algerian Water Distribution Company of Mila's governate. The annual water distribution sheets. Internal report.
- Agricultural Services Directorate of Mila (2020) Listing of use of groundwater for irrigation for the year 2019.
- Alcalá FJ, Custodio E (2008) Using the Cl/Br ratio as a tracer to identify the origin of salinity in aquifers in Spain and Portugal. *J Hydrol* 359:189–207. <https://doi.org/10.1016/j.jhydrol.2008.06.028>
- Amarouche-Yala S, Benouadah A, Bentabet A, Moulla AS, Ouarezki SA, Azbouche A (2014) Physicochemical, bacteriological, and radiochemical characterization of some Algerian thermal spring waters. *Water Qual Expo Health* 7:233–249. <https://doi.org/10.1007/s12403-014-0130-x>
- ANBT (2000) National Agency for Dams and Transfers, Algeria. Transfer of Beni-Haroun, feasibility study, financial and economic analysis, Algeria. Tractebel Engineering, p 20 (in French).
- ANRH (2003) Potential evapotranspiration map of Northern Algeria, Scale 1/500,000—Notice 1–42. Ministry of Water Resources, Algeria. (Algiers, Ed. INCT)
- ANRH (2005) Average Annual Rainfall Map of Northern Algeria, Scale 1/500,000. Water Resources, Algeria. (Algiers, Ed. INCT)
- Appelo CAJ, Postma DJ (2005) *Geochemistry, groundwater and pollution*, 2nd edn. Balkema, Rotterdam, pp 1–683. <https://doi.org/10.1201/9781439833544>
- Aquilina L, Ladouche B, Doerfliger N, Seidel JL, Bakalowicz M, Dupuy C, Le Strat P (2002) Origin, evolution and residence time of saline thermal fluids (Balaruc springs, southern France):

- implications for fluid transfer across the continental shelf. *Chem Geol* 192:1–21. [https://doi.org/10.1016/S0009-2541\(02\)00160-2](https://doi.org/10.1016/S0009-2541(02)00160-2)
- Aris Y, Coiffait PE, Guiraud M (1998) Characterisation of Mesozoic–Cenozoic deformations and palaeostress fields in the Central Constantinois, northeast Algeria. *Tectonophysics* 290:59–85. [https://doi.org/10.1016/S0040-1951\(98\)00012-2](https://doi.org/10.1016/S0040-1951(98)00012-2)
- Arnórsson S, Gunnlaugsson E, Svavarsson H (1983) The geochemistry of geothermal waters in Iceland. III. Chemical geothermometry in geothermal investigations. *Geochim Cosmochim Acta* 47:567–577. [https://doi.org/10.1016/0016-7037\(83\)90278-8](https://doi.org/10.1016/0016-7037(83)90278-8)
- Barbecot F, Marlin C, Gibert E, Dever L (1998) Identification and characterization of a saline wedge in the Bajocian–Bathonian coastal aquifer of the area of Caen (France). *Earth Planet Sci* 326:539–544. [https://doi.org/10.1016/S1251-8050\(98\)80204-8](https://doi.org/10.1016/S1251-8050(98)80204-8)
- Benabbas C (2006) Évolution Mio-Plio-Quaternaire des bassins continentaux de l’Algérie nord orientale: apport de la photogéologie et analyse morphostructurale. Doctorat d’Etat, Université de Constantine- Algeria, p 245. (in French).
- Benaouli-Mebarek N, Frizon de Lamotte D, Roca E, Bracene R, Faure JL, Sassi W, Roure F (2006) Post-cretaceous kinematics of the Atlas and Tell systems in central Algeria: early foreland folding and subduction-related deformation. *CR Geosci* 338:115–125. <https://doi.org/10.1016/j.crte.2005.11.005>
- Bishop JL, Lane MD, Dyar MD, King SJ, Brown AJ, Swayze GA (2014) Spectral properties of Ca–sulfates: gypsum, bassanite, and anhydrite. *Am Miner* 99:2105–2115. <https://doi.org/10.2138/am-2014-4756>
- Bouchaou L, Michelot JL, Vengosh A, Hsissou Y, Qurtobi M, Gaye CB, Bullen TD, Zuppi GM (2008) Application of multiple isotopic and geochemical tracers for investigation of recharge, salinization, and residence time of water in the Souss-Massa aquifer, southwest of Morocco. *J Hydrol* 352:267–287. <https://doi.org/10.1016/j.jhydrol.2008.01.022>
- Cardenal J, Benavente J, Cruz-Sanjulain J (1994) Chemical evolution of groundwater in Triassic gypsum-bearing carbonate aquifers (las Alpujarras, southern Spain). *J Hydrol* 16:3–30. [https://doi.org/10.1016/0022-1694\(94\)90119-8](https://doi.org/10.1016/0022-1694(94)90119-8)
- Castany G (1963) *Traité pratique des eaux souterraines*. 2ème éd., 410 figures, Dunod, Paris. p 696. (in French).
- Chenaker H, Houha B, Valles V (2018) Hydrogeochemistry and geothermometry of thermal water from northeastern Algeria. *Geothermics* 75:137–145. <https://doi.org/10.1016/j.geothermics.2018.04.009>
- Cherchali ME-H, Liegeois JP, Mesbah M, Moulla AS, Ouarezki SA, Daas N, Achachi A (2023) Interconnected multi-layer aquifer with evaporitic fossil waters in Chott-El-Gharbi endorheic basin (Western high plateaus, Algeria): hydrochemistry, environmental and strontium isotopes. *Appl Geochem* 148:105537. <https://doi.org/10.1016/j.apgeochem.2022.105537>
- Cidu R, Biddau R, Fanfani L (2009) Impact of past mining activity on the quality of groundwater in SW Sardinia (Italy). *J Geochem Explor* 100:125–132. <https://doi.org/10.1016/j.gexplo.2008.02.003>
- Coiffait PE (1992) Un bassin post-nappe dans son cadre structural l’exemple du bassin de Constantine (Algérie Nord Orientale). *Thèse es Sciences*. Nancy, p 502 (in French)
- Custodio E, Bruggeman GA (1987) Groundwater problems in coastal areas. *Studies and reports in hydrology*, UNESCO Publication, Tokyo, p 596
- Davis SN, De Wiest RJ (1967) *Hydrogeology*, 2nd edn. New-York, Wiley, p 463
- Demdoum A, Younes H, Feki M, Hadji R, Djebbar M (2015) Multi-tracer investigation of groundwater in El Eulma basin (North-western Algeria). *North Africa Arab J Geosci* 8:3321–3333. <https://doi.org/10.1007/s12517-014-1377-z>
- Dhaoui O, Antunes I, Boente C, Agoubi B, Kharroubi A (2023) Hydrogeochemical processes on inland aquifer systems: a combined multivariate statistical technique and isotopic approach. *Groundw Sustain Dev* 20:100887. <https://doi.org/10.1016/j.gsd.2022.100887>
- DHW Mila (1996) *Hydraulics Department of Mila. Presentation report of the Hydraulics sector*. Internal report, p 47 (In French)
- DHW Mila (2020) *Hydraulics Department of Mila. Drinking water production. Report for the year 2012* (In French)
- Dib H (2008) *Guide pratique des sources thermales de l’Est algérien*. Mém Serv Géol Natl Algér 15:1–106. (in French)
- DSASI (2021) *Agricultural statistics: areas and production*. <https://madr.gov.dz/wp-content/uploads/2022/04/SERIE-B-2019.pdf>
- Durand-Delga M (1969) *Mise au point sur la structure du Nord-Est de la Berbérie*. Serv Géol Alger NS 39:89–131
- El Achheb A, Mania J, Mudry J (2003) Mécanismes d’acquisition de la minéralisation des eaux souterraines dans le bassin Sahel Doukkala (Morocco). *Approche par des traceurs hydro-géochimiques*. IGME. Madrid 2003, pp 1–11. ISBN. 84-7840-470-8. (in French)
- Fairchild IJ, Borsato A, Tooth AF, Frisia S, Hawkesworth CJ, Huang Y, McDermott F, Spiro B (2000) Controls on trace element Sr–Mg compositions of carbonate cave waters: implications for speleothem climatic records. *Chem Geol* 166:255–269. [https://doi.org/10.1016/S0009-2541\(99\)00216-8](https://doi.org/10.1016/S0009-2541(99)00216-8)
- Farid I, Trabelsi R, Zouari K, Abid K, Ayachi M (2013) Deciphering the interaction between quaternary and continental Sabkhas aquifers in Central Tunisia using hydrochemical and isotopic tools. *Environ Earth Sci* 70:3289–3309. <https://doi.org/10.1007/s12665-013-2395-y>
- Farid I, Zouari K, Rigane A, Beji R (2015) Origin of the groundwater salinity and geochemical processes in detrital and carbonate aquifers: Case of Chougafiya basin (Central Tunisia). *J Hydrol* 530:508–532. <https://doi.org/10.1016/j.jhydrol.2015.10.009>
- Ferraga T, Pistre S (2021) Qualitative and comparative study of different methods of interpolation for the mapping of groundwater salinity: Case study of thermal waters used for irrigation in northeastern Algeria. *J Geosci Environ Prot* 9:115–132. <https://doi.org/10.4236/gep.2021.97008>
- Fontes JCh, Matray JM (1993) Geochemistry and origin of formation brines from the Paris Basin, France: 1. Brines associated with Triassic salts. *Chem Geol* 109:149–175. [https://doi.org/10.1016/0009-2541\(93\)90068-T](https://doi.org/10.1016/0009-2541(93)90068-T)
- Fournier RO (1977) Chemical geothermometers and mixing models for geothermal systems. *Geothermics* 5:41–50. [https://doi.org/10.1016/0375-6505\(77\)90007-4](https://doi.org/10.1016/0375-6505(77)90007-4)
- Fournier RO, Potter RW II (1979) Magnesium correction to the Na–K–Ca geothermometer. *Geochem Cosmochim Acta* 43:1543–1550. [https://doi.org/10.1016/0016-7037\(79\)90147-9](https://doi.org/10.1016/0016-7037(79)90147-9)
- Fournier RO, Truesdell AH (1973) An empirical Na–K–Ca geothermometer for natural waters. *Geochem Cosmochim Acta* 37:1255–1275. [https://doi.org/10.1016/0016-7037\(73\)90060-4](https://doi.org/10.1016/0016-7037(73)90060-4)
- Frape SK, Fritz RH, Mc N (1984) Water–rock interaction and chemistry of groundwaters from the Canadian Shield. *Geochim Cosmochim Acta* 48:1617–1627. [https://doi.org/10.1016/0016-7037\(84\)90331-4](https://doi.org/10.1016/0016-7037(84)90331-4)
- Gaillard J, Dupré B, Louvat P, Allègre CJ (1999) Global silicate weathering and CO₂ consumption rates deduced from the chemistry of large rivers. *Chem Geol* 159:3–30. [https://doi.org/10.1016/S0009-2541\(99\)00031-5](https://doi.org/10.1016/S0009-2541(99)00031-5)
- Giggenbach WF (1988) Geothermal solute equilibria. Derivation of Na–K–Mg–Ca geoindicators. *Geochim Cosmochim Acta* 52:2749–2765. [https://doi.org/10.1016/0016-7037\(88\)90143-3](https://doi.org/10.1016/0016-7037(88)90143-3)
- Giggenbach WF (1991) *Chemical techniques in geothermal exploration*. UNITAR/UNDP Guidebook: Application of Geochemistry in Resources Development, pp 119–144

- Grillot JC, Schoeller H (1989) Exemple d'approche pluridisciplinaire dans la caractérisation d'eaux thermales carbo-gazeuses. *Pluridiscip Approach Carbon Groundw Surv* 2:211–228. <https://doi.org/10.7202/705029ar>
- Hébrard O, Pistre S, Cheynet N, Dazy J, Batiot-Guilhe C, Seidel JL (2006) Origin of the Languedoc–Roussillon's chloride rich karstic spring waters. *C R Geosci* 338:703–710. <https://doi.org/10.1016/j.crte.2006.04.018>
- Hsissou Y, Chauve P, Mania J, Mangin A, Bakalowicz M, Gaiz A (1996) Characterization of the groundwaters of the Turonian catchment of Tadla (Morocco) by the concentration ratios of Sr^{2+} Ca^{2+} . *J Hydrol* 183:445–545. [https://doi.org/10.1016/0022-1694\(95\)03009-3](https://doi.org/10.1016/0022-1694(95)03009-3)
- Issadi A (1992) Le thermalisme dans son cadre géo-structural, apports à la connaissance de la structure profonde de l'Algérie et de ses ressources géothermales. Thèse de Doctorat d'état. IST. USTHB. Alger, p 274 (in French)
- Kedaid F (2007) Database on the geothermal resources of Algeria. *Geothermics* 36:265–275. <https://doi.org/10.1016/j.geothermics.2007.02.002>
- Khaska M, Le Gal La Salle C, Lancelot J, ASTER team, Amad M, Verdoux P, Noret A, Simler R (2013) Origin of groundwater salinity (current seawater vs. saline deep water) in a coastal karst aquifer based on Sr and Cl isotopes. Case study of the La Clape massif (southern France). *Appl Geochem* 37:0883–2927. <https://doi.org/10.1016/j.apgeochem.2013.07.006>
- Langelier WF, Ludwig HF (1942) Graphical method for indicating the mineral character of natural waters. *J Am Water Work Assoc* 34:334–335. <https://doi.org/10.1002/j.1551-8833.1942.tb19682.x>
- Lopez-Chicano M, Bouamama M, Vallejos A, Pulido-Bosch A (2001) Factors which determine the hydrogeochemical behaviour of karstic springs. A case study from the Betic Cordilleras. Spain *Appl Geochem* 16:1179–1192. [https://doi.org/10.1016/S0883-2927\(01\)00012-9](https://doi.org/10.1016/S0883-2927(01)00012-9)
- Lucas Y, Schmitt AD, Chabaux F, Clément A, Fritz B, Elsass P, Durand S (2010) Geochemical tracing and hydrogeochemical modelling of water–rock interactions during salinization of alluvial groundwater (Upper Rhine Valley, France). *Appl Geochem* 25:1644–1663. <https://doi.org/10.1016/j.apgeochem.2010.08.013>
- Martínez-Pérez L, Luquot L, Carrera J, Marazuela MA, Goyetche T, Pool M, Palacios A, Bellmunt F, Ledo J, Ferrer N, del Val L, Pezard PA, Garcia-Orellana J, Diego-Feliu M, Rodellas V, SaaltinkMW V-S, Folch A (2022) Characterizing coastal alluvial aquifers to improve understanding of seawater intrusion and submarine groundwater discharge. *J Hydrol* 607:127510. <https://doi.org/10.1016/j.jhydrol.2022.127510>
- Mebarki A (2005) Hydrologie des bassins de l'Est Algérien: ressources en eau, aménagement et environnement. Thèse de Doctorat, Université de Constantine I, Algérie, p 360 (in French)
- Moussa AB, Zouari K, Marc V (2011) Hydrochemical and isotope evidence of groundwater salinization processes on the coastal plain of Hammamet-Nabeul, north-eastern Tunisia. *Phys Chem Earth* 36:167–178. <https://doi.org/10.1007/s12665-013-2395>
- Mutlu H, Güleç N (1998) Chemical geothermometry and fluid-mineral equilibria for the Ömer-Gecek Thermal Waters, Afyon Area, Turkey. *J Volcanol Geoth Res* 80:303–321. [https://doi.org/10.1016/S0377-0273\(97\)00051-6](https://doi.org/10.1016/S0377-0273(97)00051-6)
- Nieva D, Nieva R (1987) Developments in geothermal energy in Mexico—part twelve. A cationic geothermometer for prospecting of geothermal resources. *Heat Recovery Syst CHP* 7:243–258. [https://doi.org/10.1016/0890-4332\(87\)90138-4](https://doi.org/10.1016/0890-4332(87)90138-4)
- ONM (2013) National Meteorological Office of Algeria. Average monthly rainfall and temperature data (1992–2013)
- Parkhurst DL, Appelo CAJ (2013) Description of input and examples for PHREEQC version 3-A computer program for speciation, batch-reaction, one-dimensional transport, and inverse geochemical calculations. U.S. Geol. Surv. Tech. Methods
- Piper AM (1944) A graphic procedure in the geochemical interpretation of water-analyses. *EOS Trans Am Geophys Union* 25:914–928. <https://doi.org/10.1029/TR025i006p00914>
- Powell T, Cumming W (2010) Spreadsheets for geothermal water and gas geochemistry. In: Proceedings, thirty-fifth workshop on geothermal reservoir engineering Stanford University, Stanford, California, February 1–3, 2010 SGP-TR-188
- Pulido-Bosch A, Rigol-Sanchez JP, Vallejos A, Andreu JM, Sola F (2018) Impacts of agricultural irrigation on groundwater salinity. *Environ Earth Sci* 77:1–14. <https://doi.org/10.1007/s12665-018-7386-6>
- Quinby-Hunt MS, Turehian KK (1983) Distribution of elements in sea water. *AGU Org* 64:130–130. <https://doi.org/10.1029/EO064i014p00130>
- Saibi H, Batir F, Pocasanger C (2021) Hydrochemistry and geothermometry of thermal waters from UAE and their energetic potential assessment. *Geothermics* 92:102061. <https://doi.org/10.1016/j.geothermics.2021.102061>
- Schoenherr J, Reuning L, Hallenberger M, Lüders V, Lemmens L, Biehl BC, Lewin A, Leupold M, Wimmers K, Strohmenger CJ (2018) Dedolomitization: review and case study of uncommon mesogenetic formation conditions. *Earth Sci Rev* 185:780–805. <https://doi.org/10.1016/j.earscirev.2018.07.005>
- Simler R (2014) Diagrammes. A free distribution hydrochemistry multilanguage software. Hydrogeology Lab., University of Avignon, France, v6.4
- Stigter TY, van Ooijen SPI, Post VEA, Appelo CAJ, Carvalho Dill AMM (1998) A hydrogeological and hydrochemical explanation of the groundwater composition under irrigated land in a Mediterranean environment, Algarve, Portugal. *J Hydrol* 208:262–327. [https://doi.org/10.1016/S0022-1694\(98\)00168-1](https://doi.org/10.1016/S0022-1694(98)00168-1)
- Tebbouche MY, Ait Benamar D, Hassan HM, Singh AP, Bencharif R, Machane D, Meziani AA, Nemer Z (2022) Characterization of El Kherba landslide triggered by the August 07, 2020, Mw = 4.9 Mila earthquake (Algeria) based on post-event field observations and ambient noise analysis. *Environ Earth Sci* 81:46. <https://doi.org/10.1007/s12665-022-10172-8>
- Vallejos A, Solaa F, Yechielib A, Pulido-Boscha (2018) Influence of the paleogeographic evolution on the groundwater salinity in a coastal aquifer. Cabo de Gata aquifer, SE Spain. *J Hydrol* 557:55–66. <https://doi.org/10.1016/j.jhydrol.2017.12.027>
- Van der Weijden CH, Pacheco FAL (2003) Hydrochemistry, weathering and weathering rates on Madeira Island. *J Hydrol* 283:122–145. [https://doi.org/10.1016/S0022-1694\(03\)00245-2](https://doi.org/10.1016/S0022-1694(03)00245-2)
- Vila JM (1980) La chaîne d'Algérie orientale et des confins Algéro-Tunisiens - Thèse de Doctorat es Sciences. Université de Paris. p 586 (in French)
- Walter JR, Chesnaux V, Cloutier DG (2017) The influence of water/rock–water/clay interactions and mixing in the salinization processes of groundwater. *J Hydrol Reg Stud* 13:168–188. <https://doi.org/10.1016/j.ejrh.2017.07.004>
- WHO (2008) Guidelines for Drinking Water Quality [Electronic Resource]: Third Edition, Incorporating the First and Second Addenda, Volume 1, Recommendations. World Health Organization, Geneva 1–668. <https://www.who.int/publications/i/item/9789241547611>
- Wildi W (1983) La chaîne tello-rifaine (Algérie, Maroc, Tunisie): Structure, stratigraphie et évolution du Trias au Miocène. *Rev Géol Dyn Géog Phys* 24:201–297 (in French)
- Yelles-Chaouch A, Abacha I, Boulahia O, Aidi C, Chami A, Belhouene A, Rahmani STE, Roubeche K (2021) The 13 July 2019 Mw 5.0 Jijel Earthquake, northern Algeria: an indicator of

active deformation along the eastern Algerian margin. *J Afr Earth Sci* 177:104149. <https://doi.org/10.1016/j.jafrearsci.2021.104149>

Springer Nature or its licensor (e.g. a society or other partner) holds exclusive rights to this article under a publishing agreement with the author(s) or other rightsholder(s); author self-archiving of the accepted manuscript version of this article is solely governed by the terms of such publishing agreement and applicable law.